

On improved commutation for moving-magnet planar actuators*

Yorick Broens, Hans Butler and Roland Tóth

Abstract—The demand for high-precision and high-throughput motion control systems has increased significantly in recent years. The use of moving-magnet planar actuators (MMPAs) is gaining popularity due to their advantageous characteristics, such as complete environmental decoupling and reduction of stage mass. Nonetheless, model-based commutation techniques for MMPAs are compromised by misalignment between the mover and coil array and mismatch between the ideal electromagnetic model and the physical system, often leading to decreased system performance. To address this issue, a novel improved commutation approach is proposed in this paper by means of dynamic regulation of the position dependence of the ideal model-based commutation algorithm, which allows for attenuation of magnetic misalignment, manufacturing inaccuracies and other unmodelled phenomena. The effectiveness of the proposed approach is validated through experiments using a state-of-the-art moving-magnet planar actuator prototype.

I. INTRODUCTION

In recent years, the demand for high-precision and high-throughput motion control systems has seen a significant increase across various fields, such as microelectronics, biotechnology, and nanotechnology, see [1]–[3]. To achieve highly accurate positioning of the mover while allowing for increased throughput, new electromagnetic actuator configurations with improved performance have been developed, particularly in the form of planar motors utilizing a moving-magnet configuration, see [4]–[6]. The use of *moving-magnet planar actuators* (MMPAs) is gaining popularity due to their advantageous characteristics, such as complete environmental decoupling of the mover and reduction of the stage mass, over their alternatives. However, these benefits come at the cost of introducing an additional surge of complexity from a motion control perspective due to the presence of complex nonlinear multi-physical effects that can only be approximately modeled based on first-principles knowledge, see [7]. Additional complexity arises from position dependent effects which are introduced by relative position measurements and actuation of the moving-body. To address these, coordinate frame transformations are required which accurately connect the actuation forces (stator frame) and the position measurements (metrology frame) to the specific point of control on the moving-body (translation frame), see [8].

*This work has received funding from the ECSEL Joint Undertaking (JU) under grant agreement No 875999 and from the European Union within the framework of the National Laboratory for Autonomous Systems (RRF-2.3.1-21.2022-00002).

Y.Broens, H.Butler and R.Tóth are with the Department of Electrical Engineering, Eindhoven University of Technology, Eindhoven, The Netherlands. H.Butler is also affiliated with ASML, Veldhoven, The Netherlands. R.Tóth is also affiliated with the Systems and Control Laboratory, Institute for Computer Science and Control, Hungary, (email: Y.L.C.Broens@tue.nl).

Typically, motion control design for MMPAs is simplified through the use of model-based commutation approaches, see [4]–[7]. These approaches rely on a first-principles based model of the inverse *electromagnetic* (EM) behavior of the motor, with the goal of compensating the nonlinear electromagnetic interactions between the coil array and the magnet array, thereby allowing for independent control of the mechanical *degrees of freedom* (DoFs) of the mover. However, despite the benefits of these approaches, they still require a precise characterization of the highly nonlinear behavior of the actuator, which can be difficult to obtain with sufficient accuracy due to the presence of complex nonlinear multi-physical phenomena combined with unknown manufacturing inaccuracies. Additionally, model-based commutation techniques utilized in magnetically levitated movers encounter a challenge of misalignment during system initialization due to position uncertainty of the magnetic-mover with respect to the coil array, i.e., the stator, leading to a decrease in system performance. These properties necessitate the adoption of sophisticated calibration strategies for accurate alignment of the moving-magnets with the stator to allow for high-precision positioning of the moving-body.

To address these issues, this paper presents a novel approach that allows for improving the ideal model-based commutation by calibration and active regulation of the position dependence. First, a static gradient-descent based optimization approach is investigated which provides automatic calibration of the commutation frame in terms of aligning the magnetic-mover with the coil array without the use of additional sensors. Secondly, an active regulatory approach is presented that can adapt the commutation frame to local variations of the EM relations. The latter method incorporates a secondary feedback control loop that includes a learning-based feedforward controller and a feedback controller. This loop can adapt the commutation to variations of the EM relationship due to misalignment, coil pitch, eddy currents or other manufacturing imperfections, allowing for high-precision motion performance of the mover.

The main contributions of this paper are:

- (C1) The development of a novel electromagnetic calibration approach for MMPAs by means of a gradient-descent based optimization strategy. The proposed approach allows for compensation of static misalignment of the moving-magnets with respect to the coil array.
- (C2) The development of a novel improved commutation approach which dynamically regulates the commutation frame, therefore attenuating for effects of misalignment, manufacturing inaccuracies and other remnant effects.
- (C3) The development of a position dependent learning-based

feedforward with the aim of improving the dynamic regulation of the commutation frame.

This paper is organized as follows. First, the problem formulation is presented in Section II. Next, Section III presents the proposed gradient descent based static calibration of the commutation frame, i.e., the misalignment between the moving-magnets and the coil array. Section IV introduces the proposed dynamic regulation of the commutation frame. In Section V, the design of a learning-based commutation feedforward is proposed for increasing the performance of the dynamic regulation. Section VI presents experimental results of the proposed approaches on a state-of-the-art MMPA prototype. Finally, Section VII presents the overall conclusion on the presented work.

II. PROBLEM FORMULATION

A. Background

The dynamic behavior of an MMPA system is governed by a combination of electromagnetic and mechanical phenomena, see Figure 1, resulting in a complex *multiple-input multiple-output* (MIMO) system, which exhibits position dependent effects due to the relative displacement of the mover with respect to the measurement (metrology) and actuation (stator) frames. The equations of motion, denoted by P , are given by:

$$M\ddot{q}_T^M(t) + D\dot{q}_T^M(t) + Kq_T^M(t) = HF_m(t) \quad (1)$$

where M, D and K are the symmetric mass, damping and stiffness matrices of the mover and $q_T^M(t) \in \mathbb{R}^{n_q}$ corresponds to the position vector of the mover in the metrology coordinate frame. $H \in \mathbb{R}^{n_q \times n_{F_m}}$ represents the mapping of the forces acting on the magnet plate to its center of gravity.

Assuming a *rigid-body* (RB) mover, the EM interaction, which relates the currents in the stator frame coils to forces that are exerted on the magnet plate, is given by (see [5]):

$$F_m(t) = \Omega(q_T^S(t)) i(t), \quad (2)$$

where $q_T^S(t) \in \mathbb{R}^{n_q}$ corresponds to the position vector of the mover in the stator coordinate frame. In case of misalignment between the two coordinate frames, i.e. $q_T^S = q_T^M + \Delta(q_T^M)$, the EM interaction can be reformulated as:

$$F_m(t) = \Omega(q_T^M(t) + \Delta(q_T^M(t))) i(t), \quad (3)$$

where $\Delta(q_T^M(t))$ represents the variations of the EM relationship due to misalignment, coil pitch, eddy currents and other manufacturing imperfections. Furthermore, by combining (1) and (3), the MMPA system can be represented in state-space form, denoted by \mathcal{P} , as:

$$\mathcal{P} = \left[\begin{array}{cc|c} 0 & I & 0 \\ -M^{-1}K & -M^{-1}D & M^{-1}H\Omega(q_T^M(t) + \Delta(q_T^M(t))) \\ \hline I & 0 & 0 \end{array} \right] \quad (4)$$

Note that if the position vector $q_T^M(t)$ is assumed to be fixed, (4) becomes an LTI system, which is often referred to as the *local dynamics* for a particular *frozen position* across the operating envelope of the system and is denoted by $\mathcal{P}(q)$.

It is a common practice to aim for independent control of the mechanical DoFs of an MMPA. To achieve this, rigid body decoupling methods as described in [9] are generally

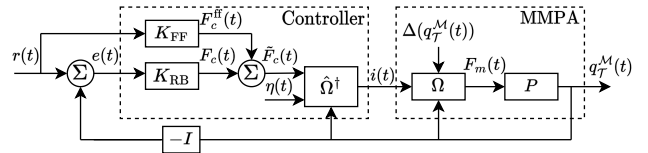


Fig. 1. Schematic representation of a control structure of an MMPA system, where $\Delta(q_T^M(t))$ describes the variations of the EM relationship due to misalignment and remnant effects of the system and $\eta(t)$ represents an additional control parameter which allows for active commutation control.

utilized. Actuator decoupling in MMPA systems is achieved through a model-based commutation algorithm, which is discussed in [4]–[6]. This algorithm aims to eliminate the input non-linearity of the system based on the inverse of the ideal EM relationship, i.e. $\Omega(q_T^M(t))\hat{\Omega}^\dagger(q_T^M(t)) = I$. However, due to the presence of misalignment of the mover in relation to the coil array, manufacturing imperfections and eddy currents, the highly nonlinear behavior of the motor may not be perfectly mitigated, resulting in a mismatch between the control forces and the physical forces acting on the mover.

We propose an approach that involves an extension of the conventional rigid body feedback control interconnection, as depicted in Figure 1, through the incorporation of a new controllable parameter $\eta(t)$. Through regulation of $\eta(t)$, we aim to minimize the following objective function:

$$\min_{\eta(t)} \left\| \Omega(q_T^M(t) + \Delta(q_T^M(t)))\hat{\Omega}^\dagger(q_T^M(t) + \eta(t)) - I \right\|, \quad (5)$$

such that effects originating from misalignment, eddy currents or other manufacturing imperfections are attenuated for, allowing high-precision motion control of the mover.

B. Problem statement

The problem that is being addressed in this paper is to develop an enhanced commutation approach which aims at eliminating the effects of $\Delta(q_T^M(t))$ through regulation of $\eta(t)$, such that the cost function expressed by (5) is minimized. We aim at developing an improved commutation approach, such that the following requirements are satisfied:

- (R1) The approach is able to establish an EM calibration of the commutation frame using local measurements, thus avoiding extensive remodelling of the EM relations.
- (R2) The approach is capable to attenuate for EM discrepancies, originating from coil pitch, eddy currents or other manufacturing imperfections.
- (R3) The closed-loop system is locally stable for *all positions* during electromagnetic calibration.

III. STATIC CALIBRATION OF THE COMMUTATION

In this section, a static EM calibration method for the commutation frame is introduced, which involves aligning the magnetic-mover with the coil array without relying on supplementary sensors. The proposed approach employs a static optimization technique to address commutation frame misalignment under the assumption that Δ is invariant with respect to q_T^M .

As the model-based commutation relies on the inverse of the ideal EM behavior of the motor, a static misalignment of the commutation frame results in static disturbance forces,

which appear in a position dependent manner due to the position dependent nature of the motor. These disturbance forces can be indirectly measured from the steady-state response of the rigid body feedback control forces as the integral action of the controller attenuates for these effects. In this context, the static attenuation forces can be viewed as a function of the position, i.e. $F_c(q_T^M + \eta)$, which can be manipulated through regulation of η . Moreover, The objective is to find the optimal calibration parameter η for commutation frame alignment, which minimizes the 2-norm of the static compensation forces across all local positions of the MMPA system. Mathematically, this is described as:

$$\min_{\eta} \sum_{i=1}^{n_p} \|F_c(q_i + \eta)\|_2, \quad (6)$$

where n_p corresponds to the number of local positions. The objective function given by (6) is reformulated into a gradient-descent (GD) based setting, see [10], [11]:

$$\Theta \eta_{k+1} = \Theta \eta_k - \lambda_k \left(\nabla \|F_c(q_1 + \eta_k)\|_2^\top \dots \nabla \|F_c(q_{n_p} + \eta_k)\|_2^\top \right)^\top, \quad (7)$$

where $k \in \mathbb{N}$ corresponds to the optimization step, λ_k is the learning rate and $\Theta = (I_{n_p \times 1} \otimes I_{n_\eta \times n_\eta})$ denotes a projection matrix. The corresponding GD optimizer is given by:

$$\eta_{k+1} = \eta_k - \lambda_k \Theta^\top \left(\nabla \|F_c(q_1 + \eta_k)\|_2^\top \dots \nabla \|F_c(q_{n_p} + \eta_k)\|_2^\top \right)^\top \quad (8)$$

In practical settings, the direct measurement of gradients is infeasible, hence an online gradient approximation method is required which capitalizes on the accessible static feedback control forces. This is achieved through $(n_\eta + 1)$ measurements per local position by introducing a perturbation parameter ξ_j with $j \in [1, n_\eta]$, thus yielding the following gradient approximation:

$$\nabla \|F_c(q_1 + \eta_k)\|_2 \approx \begin{pmatrix} \xi_1^{-1} (\|F_c(q_1 + \eta_k + \xi_1)\|_2 - \|F_c(q_1 + \eta_k)\|_2) \\ \vdots \\ \xi_{n_\eta}^{-1} (\|F_c(q_1 + \eta_k + \xi_{n_\eta})\|_2 - \|F_c(q_1 + \eta_k)\|_2) \end{pmatrix} \quad (9)$$

The resulting approach is described by Algorithm 1. The key concept is to obtain measurements of two types of control forces: (i) the averaged steady-state control forces and (ii) the averaged perturbed static control forces for all n_p local positions. These measurements are then used to reconstruct the local gradients, providing the calibration parameter update process η_{k+1} by (8). To speed up the optimization process, the step size λ_{k+1} can be updated in an

Algorithm 1 Gradient-descent based static calibration

- 1: Set initial step size λ_k
 - 2: **for** $k = 1 : n_{\text{iterations}}$ **do**
 - 3: **for** $i = 1 : n_p$ **do**
 - 4: Measure $\|F_c(q_i + \eta_k)\|_2$
 - 5: **for** $j = 1 : n_\eta$ **do**
 - 6: Measure $\|F_c(q_i + \eta_k + \xi_j)\|_2$
 - 7: **end**
 - 8: Construct $\nabla \|F_c(q_i + \eta_k)\|_2$ by (9)
 - 9: **end**
 - 10: Construct η_{k+1} by (8)
 - 11: update λ_{k+1}
 - 12: **end**
-

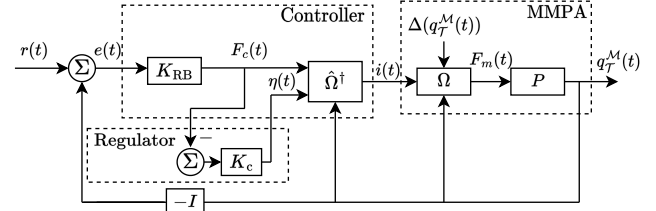


Fig. 2. Proposed feedback control interconnection for dynamic regulation of the commutation frame.

iterative manner by using line search approaches, see [11], or by considering a Gauss-Newton type approaches, e.g. using a similar strategy for Hessian approximation as (9).

IV. DYNAMIC REGULATION OF THE COMMUTATION

In this Section, a novel and enhanced commutation approach is introduced that incorporates a dynamic regulation of the commutation frame. This regulation enables the adaptation of the commutation frame to account for local variations of the EM interaction. Figure 2 illustrates the proposed dynamic regulation, in which the commutation controller K_c is designed to regulate the low-frequency content of the rigid-body feedback control forces to zero, such that the objective function, expressed by (5), is satisfied. To allow for design of K_c , the control interconnection illustrated by Figure 2 is reformulated as an LFR, see Figure 3(a), where the controllers K_{RB} and K_c are extracted into a lower connection while Ω and $\hat{\Omega}$ are lifted out as an upper connection, forming a diagonal block nonlinearity, which is denoted by $\tilde{\Delta}$. The resulting disconnected plant \tilde{P} is assumed to be a generalized plant. Moreover, under the assumption that K_{RB} robustly internally stabilizes the plant in the conventional rigid-body control case, e.g., under $K_c = 0$, see Figure 3(b), the resulting open loop transfer $r \rightarrow q_T^M$ is stable with respect to the block diagonal nonlinearity $\tilde{\Delta}$ for the full operating envelope of the system. In this context, a set of local dynamics, denoted by $\{\tilde{\Delta} \star \tilde{P} \star K_{RB}\}_{i=1}^{n_p}$, can be obtained by performing open-loop identification strategies for various forced equilibria, i.e. frozen positions, of the nonlinear system. Consequently, this set of local dynamics can be utilized for robust control design of the commutation controller K_c by means of robust sequential loop closing strategies, see [12], [13], such that closed-loop performance is improved by regulation of the commutation frame while

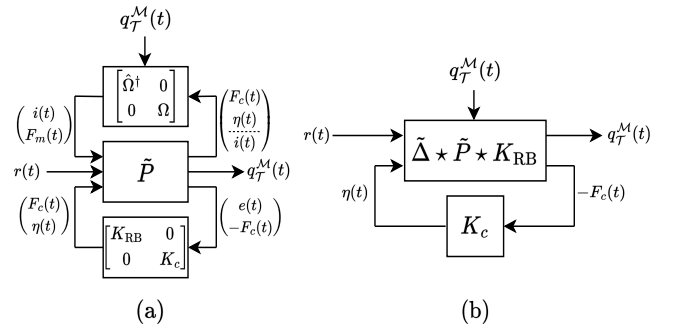


Fig. 3. Left Figure illustrates the LFR representation of the control interconnection illustrated by Figure 2. Right Figure illustrates the nonlinear plant as seen by the commutation controller K_c .

simultaneously maintaining internal stability.

Analysis of experimental data collected from a cutting-edge MMPA prototype leads to several noteworthy observations. First, it is evident that, owing to the utilization of rigid body decoupling techniques in the position control loop, all local models are decoupled at low frequencies. Secondly, the diagonal elements of the local models demonstrate a $0 \frac{dB}{dec}$ slope at low frequencies, which can be attributed to the static correlation between the compensatory control forces of the rigid body feedback controller and the relative position of the commutation frame. Therefore, the diagonal elements of the commutation controller are structured as PI-type of controllers, such that the steady-state error of the rigid body feedback control forces is actively regulated to zero by the integral action of the commutation controller. Hence, the commutation feedback controller K_c can be chosen of the form:

$$K_c = \text{diag} \left(\frac{2\pi f_{bw}^i}{s} \right), \quad i \in [1 \quad n_\eta], \quad (10)$$

where s is the complex frequency and f_{bw}^i denotes the intended commutation feedback control bandwidth, which is intentionally chosen to be 100 times smaller than *bandwidth of the position controller* to avoid excessive interaction between the two loops at high frequencies.

V. FEEDFORWARD ENHANCED DYNAMIC REGULATION

In order to enhance the performance of the dynamic regulation of the commutation frame with a more aggressive controller, a commutation feedforward controller K_c^{FF} is introduced to the control interconnection, as depicted in Figure 4. The design of the commutation feedforward can be approached in various ways. First, the solution of the gradient descent-based method, explained in section III, can be employed, thus accounting for static misalignment of the commutation frame. Alternatively, one can aim at constructing a position dependent feedforward policy that attempts to capture the spatial characteristics of $\Delta(q_T^{\mathcal{M}}(t))$ in terms of learning the mapping of $q_T^{\mathcal{M}} \rightarrow \eta$. To construct such a feedforward, n experiments are conducted with the aim of constructing a dataset \mathcal{D}_n , which consists of locally optimized parameter vectors as a function of the position, i.e. $\mathcal{D}_n = \{\eta^*(i), x_T^{\mathcal{M}}(i), y_T^{\mathcal{M}}(i)\}_{i=1}^n$. Moreover, this dataset is obtained by assessing the output of the dynamic regulator K_c at n local positions, which is facilitated by the integral action of the commutation controller. Figure 5 illustrates the experimental findings in terms of its η_x^* and η_y^* components,

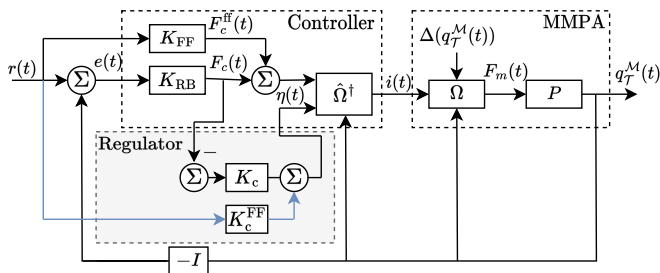


Fig. 4. Proposed dynamic regulation of the commutation frame using commutation feedback controller K_c and feedforward controller K_c^{FF} .

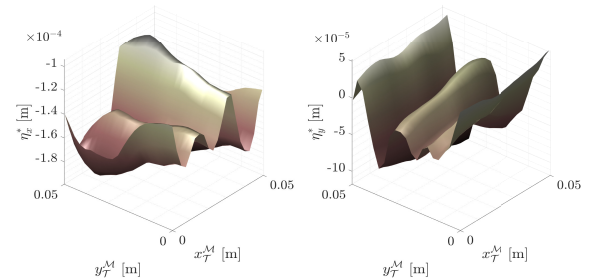


Fig. 5. Optimized $\{\eta_t^*(i)\}_{i=1}^N$ in terms of its x and y components, obtained from experiments using a state-of-the-art MMPA prototype.

revealing various noteworthy observations. Primarily, a static misalignment of the commutation frame is evident, as inferred by the non-zero mean of the optimized parameters. Secondly, it is observed that the spatial behavior is dominated by nonlinear effects, which can be attributed to coil pitch, eddy currents, and other unmodelled EM relations.

To estimate the EM discrepancies $\Delta(q_T^M)$ based on the outcomes of these local experiments, we adopt the *Gaussian Process* (GP) framework, which offers a number of practical benefits compared to other techniques, including lookup tables and artificial neural networks. First, the GP framework provides confidence bounds on the posterior estimate, ensuring the accuracy of the corresponding learning-based estimator. Additionally, the GP framework is able to effectively model nonlinear mappings through appropriate kernel selection, which has been demonstrated to be effective in practical settings, see [14]–[16]. Using the GP framework, the local variations of the EM relations are modelled as:

$$\eta_m^*(i) = \Delta_m(w(i)) + \epsilon(i), \quad \text{with } \epsilon \sim \mathcal{N}(0, \sigma_\epsilon^2), \quad (11)$$

where i corresponds to the time index, η_m^* denotes the m -th element of the η^* vector and ϵ is assumed to be independent and identically distributed (i.i.d.) white Gaussian noise with variance σ_ϵ^2 , see [17]. The local commutation frame discrepancies Δ_m are parameterized by an input vector $w(i)$, where $w(i) = [x_{\mathcal{T}}^{\mathcal{M}}(i) \ y_{\mathcal{T}}^{\mathcal{M}}(i)]^\top$, and are modelled as a GP following the approach presented in [18] as:

$$\Delta_m(w) \sim \mathcal{GP}(0, \kappa_m(w, w')) \quad (12)$$

where the covariance is fully characterized by the kernel functions $k_m(w, w')$. Moreover, the joint Gaussian distribution of the observed target values $\{\eta_m^*(i)\}_{i=1}^n$ and the commutation frame discrepancies for a given test input $w^* \in \mathbb{R}^2$ is given by:

$$\begin{bmatrix} \{\eta_m^*(i)\}_{i=1}^n \\ \Delta_m(w^*) \end{bmatrix} \sim \mathcal{N}\left(0, \begin{bmatrix} \kappa_m(W, W) + \sigma_\epsilon^2 I & \kappa_m(W, w^*) \\ \kappa_m^\top(W, w^*) & \kappa_m(w^*, w^*) \end{bmatrix}\right), \quad (13)$$

where $W \in \mathbb{R}^{2n}$ corresponds to the observed input data points of \mathcal{D}_n . Based on \mathcal{D}_n , the predictive a posteriori distribution computed from (13) is given by:

$$\hat{\Delta}_m(w^*) \triangleq \mathbb{E}\{\Delta_m(w^*)|\mathcal{D}_n, w^*\} = \Psi\{\eta_m^*(i)\}_{i=1}^n, \quad (14)$$

$$\text{cov}\{\Delta_m(w^*)|\mathcal{D}_n, w^*\} = \kappa_m(w^*, w^*) - \Psi\kappa_m(W, w^*)$$

where:

$$\Psi = \kappa_m^\top(W, w^*)(\kappa_m(W, W) + \sigma_\epsilon^2 I)^{-1} \quad (15)$$

Moreover, the construction of the feedforward controller K_c^{FF} involves using the mean of the *posterior GP distribution*, leading to a diagonal Gaussian process-based feedforward control strategy:

$$K_c^{\text{FF}} = \text{diag}(\{\hat{\Delta}_m(w^*)\}_{m=1}^{n_\eta}) \quad (16)$$

where it is reasonable to assume that the test input is $w^* \approx [r_x \ r_y]^\top$. Based on this assumption, the Gaussian process-based estimator can be employed as a feedforward controller, as depicted in Figure 4.

Achieving a precise and reliable estimator $\hat{\Delta}_m$ hinges on the careful selection of the kernels $k_m(w, w')$, which determine the *Hilbert space* within which the mean of (14) is searched for as a true estimate of $\Delta(q_T^M)$. In light of the experimental findings presented in Figure 5, we propose the adoption of the following kernel selection as a baseline approach:

$$k_m(w, w') = \sigma_{m_1}^2 \exp \left(- \sum_{v=1}^2 \frac{\|w_v - w'_v\|_2^2}{\sigma_{m_{v+1}}^2} - \sum_{v=1}^2 \frac{2 \sin^2 \left(\frac{w_v - w'_v}{2} \right)}{\sigma_{m_{v+3}}^2} \right), \quad (17)$$

where w_v corresponds to the v_{th} element of the input vector, i.e. $[x_T^M \ y_T^M]^\top$. The proposed baseline kernel is composed of a combination of a periodic kernel [19] and a radial basis function kernel [20]. The former kernel accounts for the manufacturing inaccuracies and higher harmonics, while the latter captures the non-linear residual EM effects that were not incorporated in the ideal model-based commutation.

The proposed kernel functions, given by (17), are characterized by 6 hyper-parameters, namely $[\sigma_{m_1}^2 \ \dots \ \sigma_{m_5}^2 \ \sigma_\epsilon^2]^\top$. These parameters are tuned to suit the specific estimation problem by adjusting the Hilbert space accordingly. Hence, the variance σ_ϵ^2 is jointly optimized with the kernel hyperparameters. The computation of these hyperparameters is carried out via the maximization of the marginalized likelihood, using the available training set \mathcal{D}_n , as outlined in [21]. For validation of the GP-based estimators, the Best Fit Ratio (BFR) is used, see [22], which is given by:

$$\text{BFR} = 100\% \cdot \max \left(1 - \frac{\|\{\eta_m^*(i)\}_{i=1}^n - \{\hat{\Delta}_m(w(i))\}_{i=1}^n\|_2}{\|\{\eta_m^*(i)\}_{i=1}^n - \bar{\eta}_m^*\|_2}, 0 \right), \quad (18)$$

where $\bar{\eta}_m^*$ corresponds to the sample mean of $\{\eta_m^*(i)\}_{i=1}^n$. Table I presents the BFR results of the GP-based feedforward in terms of its x and y components, relative to both its training dataset \mathcal{D}_n and a novel validation dataset. The findings indicate that the proposed baseline kernels, namely the combination of a periodic kernel and a radial basis function kernel, enable the GP-based estimator to accurately capture the local discrepancies of the EM relationships, thus rendering it a reliable commutation feedforward controller.

TABLE I

VALIDATION OF ESTIMATED GP-BASED FEEDFORWARD ON A VALIDATION SET.

	Training data set	Validation data set
BFR $\Delta_x(w^*)$ [%]	89.80	85.18
BFR $\Delta_y(w^*)$ [%]	84.84	83.34

VI. EXPERIMENTAL VALIDATION

A. MMPA prototype system

The MMPA system, depicted in Figure 6, consists of three main components: a stator base on which a double layer coil array is mounted, a lightweight translator on which a Hallbach array, comprised of 281 permanent magnets, is mounted, and a metrology frame on which 9 laser interferometers are mounted to measure the relative displacement

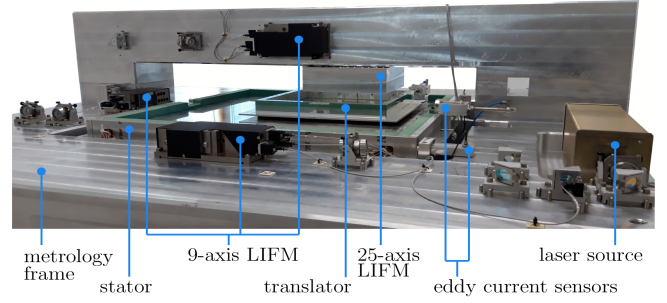


Fig. 6. Photograph of a moving-magnet planar actuator system prototype.

of the translator with respect to the metrology frame. The double layer coil array of the stator base consists of 160 coils of which 40 coils are simultaneously activated at every time instant using 40 power amplifiers, allowing for levitation and propulsion of the magnet plate in 6 DoF. For a more comprehensive description of the MMPA prototype, readers can refer to [23].

B. Experimental results

To illustrate the functionality of the proposed approaches, i.e. static calibration of the commutation frame (Section III) and GP-feedforward enhanced dynamic regulation of the commutation frame (Section IV-V), time-domain experiments have been performed on the MMPA prototype. For implementation of the proposed approaches on the experimental prototype, the static EM calibration approach, presented in Section III, was employed based on 36 local positions, leading to an optimal static commutation frame alignment parameter. For implementation of the GP-feedforward enhanced dynamic regulation of the commutation frame, the GP-based feedforward, discussed in Section V, is implemented in conjunction with the dynamic regulation proposed in Section IV. The commutation feedback controllers are designed based on (10), where the bandwidth of the commutation feedback controllers is set to be 100 times smaller than the bandwidth of the corresponding controllers of the position loop.

To assess performance in lithographic applications, the Moving-Average (MA) performance metric is introduced, see [3], which allows to analyse the low-frequent spectral content of the position tracking error during the lithographic exposure process, which takes place in the constant velocity interval of the motion profile. The MA performance metric is given by:

$$\text{MA}(t) = \frac{1}{T} \int_{t-\frac{T}{2}}^{t+\frac{T}{2}} e(\tau) d\tau, \quad (19)$$

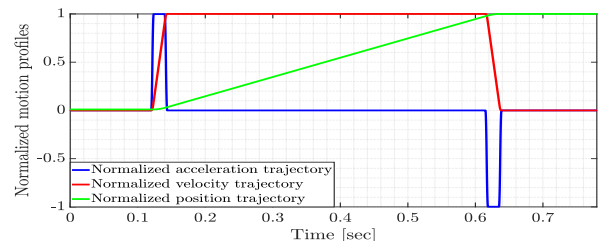


Fig. 7. Normalized motion profiles considered for experimental validation, where $a_{\max} = 5 \frac{m}{s^2}$, $v_{\max} = 0.1 \frac{m}{s}$ and $x_{\max} = 0.05m$.

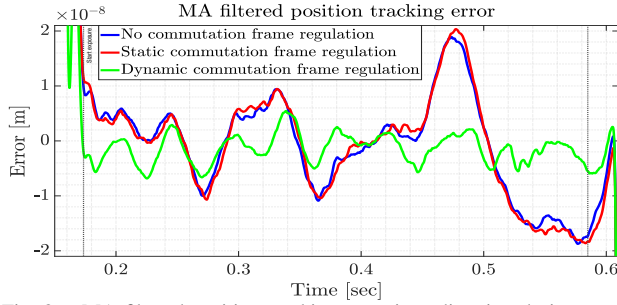


Fig. 8. MA filtered position tracking error in y -direction during constant velocity interval of the motion profile with: (—) No commutation control, (—) Static regulation of the commutation frame (Section III) (—) Dynamic regulation of the commutation frame (Section IV) combined with a learning-based commutation feedforward (Section V).

where e corresponds to the raw position tracking error and $T = 0.0144s$ is the exposure time of a single point on the wafer. For experimental validation of the proposed approaches, a lithographic scanning motion is performed in the y_T^M direction using the normalized motion profiles presented in Figure 7, where $a_{\max} = 5 \frac{m}{s^2}$, $v_{\max} = 0.1 \frac{m}{s}$, and $x_{\max} = 0.05m$. The experimental results, e.g. the MA filtered position tracking errors in y_T^M -direction during the constant velocity interval of the motion profile, are illustrated in Figure 8. Specifically, the blue graph depicts the position tracking error in of the conventional rigid body control structure, the red graph shows the position tracking error using the proposed static EM alignment approach and the green graph corresponds to the position tracking error of the proposed GP-feedforward enhanced dynamic regulation of the commutation frame. Based on Figure 8, several observations can be made. First, the static calibration approach proposed in Section III is not sufficient at improving position tracking performance. This can be explained by the behavior of $\Delta(q_T^M)$, which is dominated by nonlinear effects that can be attributed to coil pitch, eddy currents and other manufacturing imperfections as illustrated in Figure 5. Secondly, it is observed that implementation of the GP-feedforward enhanced dynamic regulation of the commutation frame improves the peak MA error from ≈ 18.7 nm to ≈ 6.6 nm, resulting in a relative reduction of the peak MA error of 64.71%, thus illustrating the potential of the proposed approach in terms of improving the EM relations of the ideal model-based commutation algorithm.

VII. CONCLUSIONS

This paper introduces a methodology to enhance the ideal model-based commutation by regulating the commutation frame both statically and dynamically, thereby aiming at minimization of the cost function expressed by (5). It is found that the static optimization of the commutation frame is not sufficient in terms of improving the position tracking performance of the MMPA prototype, as it does not account for the highly nonlinear EM behavior induced by coil pitch, eddy currents, and other unmodelled EM effects. Nonetheless, the GP-feedforward enhanced dynamic regulation of the commutation frame demonstrates great potential as it reduces the peak MA error by 64.71% compared to conventional

rigid body control interconnection. This is achieved by the GP-based feedforward's ability to effectively capture the nonlinear behavior of the EM relations, in combination with the integral action of the dynamic regulation, which effectively attenuates any possible EM misalignment, thus enabling high-precision motion control of the mover.

REFERENCES

- [1] L. Y. Zhang, J. Gao, and H. Tang, "Development and modeling of a macro/micro composite positioning system for microelectronics manufacturing," in *Proc. of the Key Engineering Materials*, vol. 679, pp. 135–142, Trans Tech Publ, 2016.
- [2] T. Qu, J. Chen, S. Shen, Z. Xiao, Z. Yue, and H. Y. Lau, "Motion control of a bio-inspired wire-driven multi-backbone continuum minimally invasive surgical manipulator," in *Proc. of the 2016 IEEE International Conference on Robotics and Biomimetics (ROBIO)*, pp. 1989–1995, IEEE, 2016.
- [3] H. Butler, "Position control in lithographic equipment [applications of control]," *IEEE Control Systems Magazine*, no. 5, pp. 28–47, 2011.
- [4] I. Proimadis, *Nanometer-accurate motion control of moving-magnet planar motors*. PhD thesis, Department of Electrical Engineering, 2020.
- [5] J. M. M. Rovers, *Multiphysical modeling of high-precision electromechanical devices*. PhD thesis, Eindhoven University of Technology, 2013.
- [6] C. M. M. van Lierop, *Magnetically levitated planar actuator with moving magnets: Electromechanical analysis and design II*. PhD thesis, Eindhoven University of Technology, 2007.
- [7] J. M. M. Rovers, J. W. Jansen, and E. A. Lomonova, "Multiphysical analysis of moving-magnet planar motor topologies," *IEEE Transactions on Magnetics*, vol. 49, no. 12, pp. 5730–5741, 2013.
- [8] M. Steinbuch, "Design and control of high tech systems," in *Proc. of the 2013 IEEE ICM*, pp. 13–17, 2013.
- [9] M. Steinbuch and M. Norg, "Advanced motion control: An industrial perspective," *European Journal of Control*, pp. 278–293, 1998.
- [10] S. Ruder, "An overview of gradient descent optimization algorithms," *arXiv preprint arXiv:1609.04747*, 2016.
- [11] E. Berglund, *Novel Hessian approximations in optimization algorithms*. PhD thesis, KTH Royal Institute of Technology, 2022.
- [12] T. Oomen, "Advanced motion control for precision mechatronics: control, identification, and learning of complex systems," *IEEE Journal of Industry Applications*, vol. 7, pp. 127–140, Jan. 2018.
- [13] S. Skogestad and I. Postlethwaite, *Multivariable feedback control: analysis and design*, vol. 2. 2007.
- [14] I. Proimadis, Y. Broens, R. Tóth, and H. Butler, "Learning-based feedforward augmentation for steady state rejection of residual dynamics on a nanometer-accurate planar actuator system," in *Proc. of the Learning for Dynamics and Control*, pp. 535–546, PMLR, 2021.
- [15] M. Poot, J. Portegies, N. Moeren, M. van Haren, M. van Meer, and T. Oomen, "Gaussian processes for advanced motion control," *IEEE Journal of Industry Applications*, vol. 11, no. 3, pp. 396–407, 2022.
- [16] M. van Meer, G. Witvoet, and T. Oomen, "Optimal commutation for switched reluctance motors using gaussian process regression," *IFAC-PapersOnLine*, vol. 55, no. 37, pp. 302–307, 2022. 2nd Modeling, Estimation and Control Conference MECC 2022.
- [17] F. M. Dekking, C. Kraaikamp, H. P. Lopuhaä, and L. E. Meester, *A Modern Introduction to Probability and Statistics: Understanding why and how*, vol. 488. Springer, 2005.
- [18] C. K. Williams and C. E. Rasmussen, *Gaussian processes for machine learning*, vol. 2. MIT press Cambridge, MA, 2006.
- [19] D. J. MacKay *et al.*, "Introduction to gaussian processes," *NATO ASI series F computer and systems sciences*, vol. 168, pp. 133–166, 1998.
- [20] R. M. Neal, *Bayesian learning for neural networks*, vol. 118. Springer Science & Business Media, 2012.
- [21] C. E. Rasmussen, C. K. Williams, *et al.*, *Gaussian processes for machine learning*, vol. 1. Springer, 2006.
- [22] A. Simpkins, "System identification: Theory for the user, (Ijung, I.; 1999)[on the shelf]," *IEEE Robotics & Automation Magazine*, vol. 19, no. 2, pp. 95–96, 2012.
- [23] I. Proimadis, C. H. Custers, R. Tóth, J. Jansen, H. Butler, E. Lomonova, and P. M. Van den Hof, "Active deformation control for a magnetically levitated planar motor mover," *IEEE Transactions on Industry Applications*, vol. 58, no. 1, pp. 242–249, 2021.